Experiments in Fluids (2022) 63:146
https://doi.org/10.1007/s00348-022-03493-8

RESEARCH ARTICLE

Improving performances of biomimetic wings with leading-edge tubercles

Giorgio Moscato[1] · Jais Mohamed[1] · Giovanni Paolo Romano[1]

Received: 12 April 2022 / Revised: 7 July 2022 / Accepted: 28 July 2022

Abstract

The present study aims investigating experimentally wing/blade geometries in which the leading edge is modified by the presence of artificial bumps, following examples in nature ("biomimetics"). Specifically, the tubercles observed in humpback whales are considered with a special focus on easy manufacturing and performance improvements, trying to overcome the observed lift coefficient reduction before stall in comparison with a standard wing. To this end, different tubercle geometries are tested, by measuring overall forces acting on the wings and by deriving detailed velocity fields using particle image velocimetry. Measurements indicate performance improvements for all trailing edge tubercle geometries here tested. In addition, the detailed analysis of mechanisms underlying the improvement of performances suggests that a triangular shape of the leading edge combines the advantages of easy manufacturing and improvements of pre-stall behaviour. So far, a simple mathematical model, describing tubercles as delta wings, is presented and verified by experimental data. The objective of the present work is focusing on the basic fluid-mechanics phenomena involved, to show that beneficial effects of tubercles are present even when tubercle details are simplified, in order to couple performance improvement and ease of assembly.

Graphical Abstract

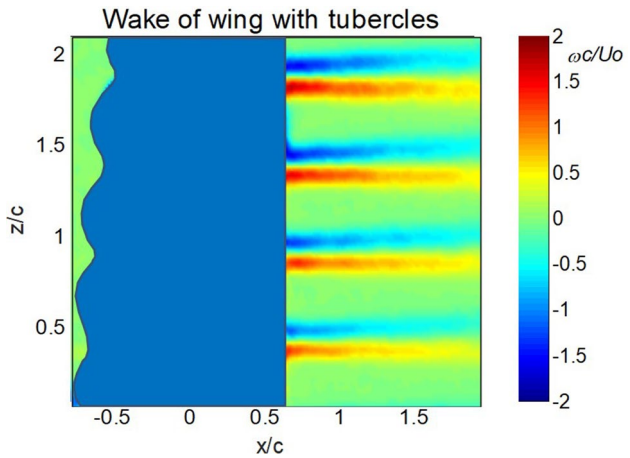

1 Introduction

Among all cetaceans, the humpback whale is the one who has the higher capability to perform underwater acrobatic trajectories, in addition to the well-known ability to perform jumps out of the water (Fig. 1). Indeed, the Latin name "megaptera novaeangliae" just has the suggestive meaning of "giant wings of New England". The whale short-range

✉ Giovanni Paolo Romano
giampaolo.romano@uniroma1.it

[1] University of Rome Sapienza, Rome, Italy

Published online: 30 August 2022

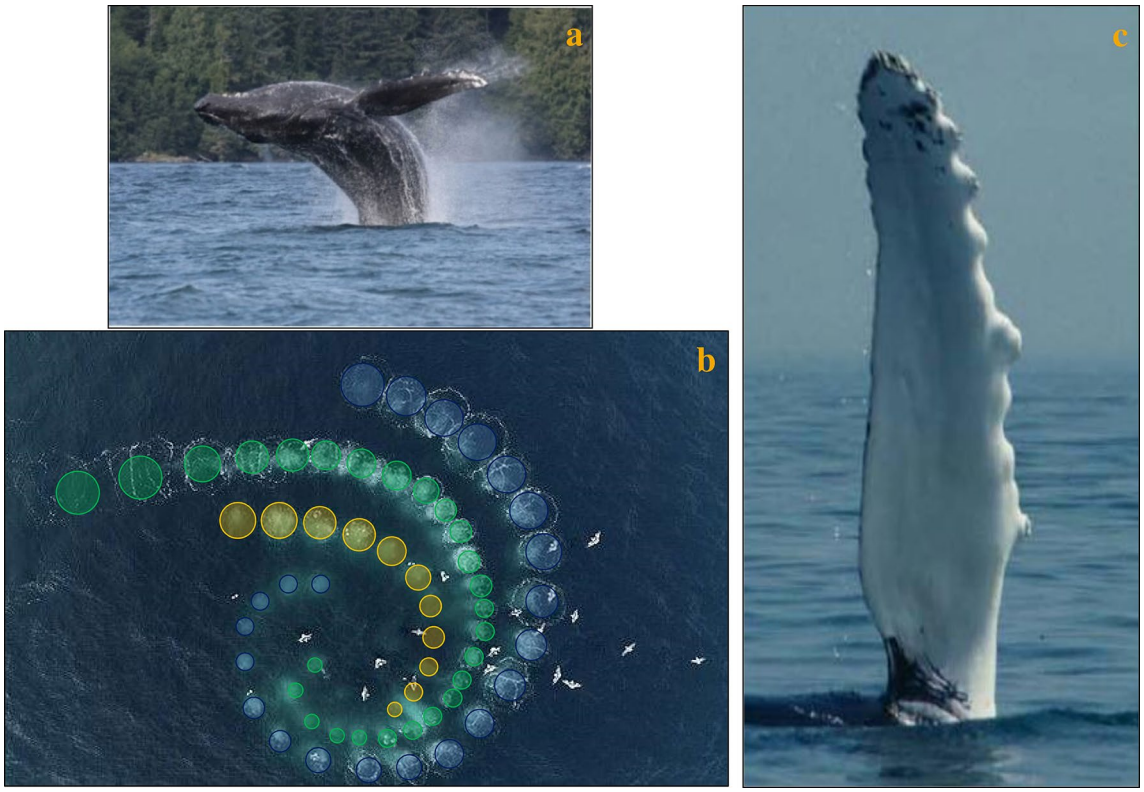

Fig. 1 An example of humpback whale jump (**a**) (Segre et al. 2020) and of bubble feeding hunting technique as revealed by air bubbles released by three cooperating whales and by the resulting trajectories on the free surface (in blue, green, and yellow (**b**). The effective whale flipper with tubercles (**c**) (Fish and Lauder 2006)

manoeuvres are used to trap preys as krill, other crustaceans and salmons, as reported in Fig. 1 (Fish and Lauder 2006). This outstanding skill is basically dependent on the long flippers, which are as long as 5 m, *i.e.* the longest appendages of any animal, and are moved quite easily independently one from the other. The distinctive feature of such flippers is the presence of several bumps along the leading edge, called tubercles, leading to an irregular wavy leading edge as reported in Fig. 1.

From the observations of the high cooperative behaviour of several specimens in hunting preys, investigations started to understand if those flippers were responsible for most of this high manoeuvrability and of related skills (Miklosovic et al. 2004; Kosma et al. 2019). Specifically, the important question to be solved was if a wing model equipped with tubercles was able to delay wing stall and to attain higher lift in comparison with a standard wing. The obtained results indicated that in certain working conditions, wing performances are indeed increased, so that biomimetic engineering applications seem to be possible (Anders 2000; Miklosovic et al. 2007; Choi et al. 2012; New and Ng 2020).

So far, a significant interest has grown towards the possible use of tubercles in technological devices to improve performances both in water and in air, still keeping manufacturing as easy as possible. The straightforward applications of such tubercle wings are in water, *i.e.* for rudders, keels, fins, propellers (Fish et al. 2011; Jansen and Nilsson 2017; Shanmukha Srinivas et al. 2018), tidal turbines (Shi et al. 2016), but also in air on wings (Zhan et al. 2014; Chen and Wang 2014; Bolzon et al. 2016), on using plasma actuators (Meng et al. 2019; Pendar and Pascoa 2022), cavity flows (Li et al. 2020; Pendar 2020), fans (Corsini et al. 2013), car aerodynamic components, Micro Air Vehicles (MAV) (Zhang et al. 2014) and small-scale wind turbines (Fish et al. 2011). Surprisingly, the most interesting application is just the last one, because in comparison with a standard blade, those with tubercles ensure higher performances in case of low-intensity winds, relatively small Reynolds numbers, on a large interval of angles of attack, in presence of turbulent flows, with also a possible reduction in noise emission (Fish et al. 2011; Zhang et al. 2014; Shi et al. 2016)).

Improvements of tubercle wing performances, specifically lift increments, have been reported by Watts and Fish 2001, whereas Miklosovic et al. 2004, reported an effective increase in the angle of stall and a smoother behaviour of lift after stall in comparison with the sudden decrease observed in wings without tubercles. Watts and Fish 2001

underlined the problem of decreasing induced drag, which it is still a matter of discussion being related to the strong three-dimensional nature of the phenomenon (Miklosovic et al. 2007; Stanway 2008; Hansen et al. 2011; Rostamzadeh et al. 2013, 2014).

To this end, it is important to distinguish between investigations made on two-dimensional arrangements, *i.e.* full-span aerofoil sections, and finite-span three-dimensional planforms, also in respect to possible interactions of the vortex system generated by tubercles with tip vortices. The investigation of full-span geometries mainly focused on sinusoidal leading-edge tubercles, so far trying to optimize performances in terms of tubercle wavelength and amplitude (Johari et al. 2007; Hansen et al. 2011; de Paula et al. 2017; Chaitanya et al. 2017; New and Ng, 2020). Apart from some difference due to the specific geometry, the overall emerging picture is that as smaller are tubercle wavelength (λ) and amplitude (A) as better performances are obtained in terms of high stall angle, maximum lift coefficient, and drag reduction. However, a minimum value for the wavelength has been determined, around 1/5 of the chord, to retain these advantages (Hansen et al. 2011). Presumably, this is due to the fact that in case of very small wavelengths, the modification of the flow field due to tubercles is not sufficient to overcome the separation occurring at stall. On the other hand, large amplitudes give rise to a smoother stall behaviour in comparison with the unmodified aerofoil. These observations pointed out the role of the amplitude to wavelength ratio, A/λ, with best performances attained for a value $A/\lambda \approx 0.55$, when vortices generated at the leading edge maintain closer one to each other and more likely interact (Hansen et al. 2011). However, the increment of performances in comparison with those of standard aerofoils is not achieved over a wide range of angles of attack and this is a particularly severe limitation.

Regarding finite-span configurations, which surely are more relevant for applications, again tubercle spacing and amplitude were found to be relevant, but in this case the phenomena must be considered both at each spanwise location and over the whole wing, as for example by considering the distribution of tubercles along the span, the alignment of tubercles to the mean flow and possible swept angle effects (Hansen et al. 2010; Custodio et al. 2015). Again, disregarding minor differences due to different geometries, wings with tubercles of small amplitude and wavelength usually performed better than standard wings. Numerical genetic algorithms tried to extract more general behaviours by focusing on variations of amplitude, amplitude to root chord ratios (van Nierop et al. 2008), spacing, location, and phase of tubercles (Bolzon et al. 2016, 2017). Results obtained for variable amplitude and phase indicated lift smoothing close to stall, stall delay, with a counterpart in maximum lift decrement, with a significant insensitivity to changes in wavelength. This appears to be in partial contrast with results from full-span investigations and surely asks for further evidence. Regarding the effect of swept wing and the alignment with the free stream, best performances were obtained for tubercles aligned with the leading edge, *i.e.* almost orthogonal to the mean flow (Wei et al. 2017).

Additional problems which limit the widespread applications of tubercle wings are related to geometrical complexity and pre-stall behaviour. The first problem is associated with the rather complex geometry of tubercles, and to their specific details as shape and curvature, which could prevent easy manufacturing. The basic question is if this complexity was really an essential requirement for improving performances or if the overall picture was the same whatever the geometrical details.

From the analysis of previously reported investigations, it seems that the flow mechanisms leading to performance enhancements were all similar between them, even in wings with simple wavy leading edges (Rostamzadeh et al. 2013). Therefore, it seems that even simple wing leading-edge shapes, for example triangular, *e.g.* a sort of small delta wing, could lead to performance improvements (Custodio 2007; Fish et al. 2011) and these solutions should be detailed even more.

Regarding pre-stall behaviour, as previously reported, many investigations agree on a more gradual stall, delayed at a higher angle of attack when tubercles are employed in comparison with standard wings. However, there is not an overall agreement in pre-stall region, where sometimes a strong reduction of lift and aerodynamic efficiency was found, *i.e.* more than 20% (Johari et al. 2007; van Nierop et al. 2008; Zhang et al. 2014). To determine a possible solution to this problem, it must be considered that the major origin for the superior post-stall performances of tubercle wings has been ascribed to the different behaviours of the incoming flow on peaks and troughs (Hansen et al. 2011, 2016; Rostamzadeh et al. 2013, 2014). In those references, also using flow visualizations and local pressure measurements, the authors have shown that while at pre-stall, cross sections over troughs contribute to lift generation more than peaks, at post-stall the opposite taking place. Indeed, the model described by van Nierop et al. 2008, based on Prandtl's lifting-line theory, indicates that flow separation mostly occurs at troughs, with the formation of counter-rotating vortex pairs. So far, it seems that modifications of the bound circulation originated by tubercles are the key to improve performances at pre-stall regimes. These findings have been pointed out even more clearly in the case of delta wings with tubercles (Goruney and Rockwell 2009). So far, one of the objectives of this work is to verify the possibility of explaining the performances of tubercled wings by considering a sort of delta wing analogy, using pairs of counter-rotating vortices.

In this paper, following Rostamzadeh et al. 2013, 2014, wavy leading-edge wings are investigated, trying to overcome the limitation of lift coefficient reduction before stall in comparison with a standard wing. The analysis of the mechanisms underlying the improvement of performances, suggests that a shape of the wavy leading edge similar to a sequence small delta wings ensure improving pre-stall regime behaviour, still keeping the other regime unchanged (Custodio 2007; Fish et al. 2011; Chen and Wang 2014). Specifically, among the two solutions proposed by Rostamzadeh et al. 2013, one in which the geometrical angle of attack changes as a sinusoid in the spanwise direction without tubercles and another with tubercles, where the chord varies in a sinusoidal manner along the span, here two different possibilities are investigated. In the first the tubercles are replaced by evenly spaced sort of triangular shapes, which have the advantage of a much easier manufacturing, in the second the tubercles are non-uniformly spaced along the span, with variable wavelength and amplitude. The objective of the present work is to show beneficial effects of tubercles even when tubercle details are simplified, in order to couple performance improvement and ease of assembly. Secondly, a simple model describing tubercles as delta wings is presented and verified by experimental data.

2 Experimental set-up

Three wing models have been tested in the subsonic wind tunnel of the Mechanical and Aerospace Engineering Department at University La Sapienza, where x is the streamwise direction starting from mid-wing location, y is the vertical from the pivot point at the leading edge, $y=0$ being taken on the wing surface and z is taken along the span starting from the root. The circular open test section has a diameter of 1 m and a length of 1.5 m, the free-stream velocity being variable between 5 and 40 m/s, with a background turbulent intensity equal to 0.3% at 15 m/s. The different wings are shown in Fig. 2 and have the following features:

- Wing model without tubercles to be used for comparison (standard wing);
- Wing model with tubercles with smoothed triangular shape, with constant wavelength and amplitude along the wing span (wing with constant tubercles);
- Wing model with tubercles with wavelength and amplitude decreasing from the root to the tip (wing with variable tubercles).

Dotted lines in Fig. 2 indicate the standard wing planform as overlapped to the tubercled wings. All three models are made of an alloy Aluminium Anticorodal 6082, with same half-span, equal to 0.4 m, root chord, $c_r=0.1$ m, tip chord, equal to 0.025 m, thickness equal to $c_r/6$ up to half chord and then linearly decreasing to 0 towards the trailing edge, and weight, around 1.17 kg each. The aspect ratio is 4 and the planform area is equal to 0.035 m^2. As in Miklosovic et al. 2004, the tubercle leading edge started from 1/4th of the span, in comparison with the standard wing which has an elliptic leading edge. The main differences are that the apical part of each tubercle has a triangular shape rather than to be strictly sinusoidal, as can be noticed from Fig. 2. In the first tubercle wing, the amplitude is constant and equal to $A=0.01$ m ($\eta=A/c_r=0.1$), as also the wavelength, equal to

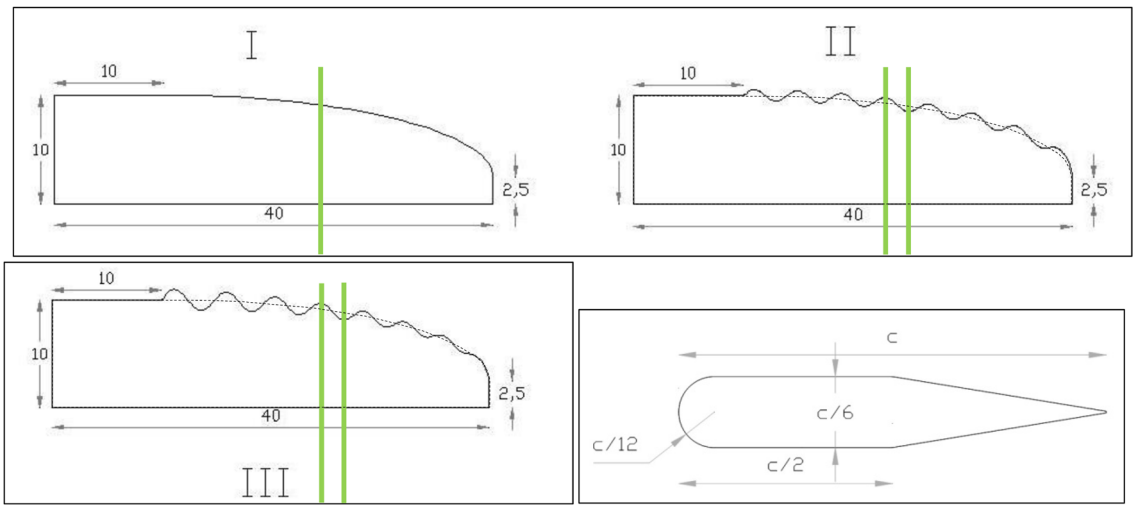

Fig. 2 The three tested wing model planforms and cross section: wing without tubercles (I), wing with tubercles of constant amplitude and wavelength (II), and wing with variable tubercles (III). Airfoil cross section used for all wings (at the bottom right). All dimensions are given in centimetres and c is the local chord. The green lines indicate locations of PIV vertical measurement planes

$\lambda = 0.04$ m ($= 0.4\ c_r$). On the other hand, in the second wing model, the amplitude is variable from 0.02 m ($\eta = 0.2$) at 1/4th span to 0.005 m ($\eta = 0.05$) at the tip, whereas the wavelength changes from 0.05 to 0.035 m (from 0.5 to 0.35 c_r) again along the span. For comparison, according to Fish and Battle 1995, a typical whale has $\eta = 0.06$. The ratio among the amplitude and the wavelength of the tubercles, A/λ is ranging from $A/\lambda = 0$ (standard wing), to $A/\lambda = 0.25$ (wing with constant tubercles) and A/λ in the range 0.15–0.4 (wing with variable tubercles). It is important to notice that for the second model this value is close to that of Johari et al. 2007, whereas for the third it is closer to that indicated by Hansen et al. 2011.

The wing section is a simplified airfoil with semi-circular rounded leading edge, followed by plane upper and lower surfaces up to 50% of the chord and then by a linear cut towards the trailing edge, as indicated specifically in Fig. 2. Again this choice is driven by the idea to simplify as much as possible the manufacturing process and to show that even for these non-optimal airfoil geometries (Guan et al. 2016) the positive impact of a tubercle leading edge is high.

For each model, the free-stream velocity was selected to 30 m/s, so that the Reynolds number, based on the wing chord was around 2×10^5. For comparison, the Reynolds number of a swimming whale in the sea is around 2×10^6 with typical chord of the flipper around 1 m and velocities around 3 m/s. Being the wind tunnel test section cross area equal to about 0.75 m^2, the solid blockage error due to the wing model volume (around 4×10^{-4} m^3) is evaluated to be less than 0.1% (Pope and Harper 1966). Similarly, the wake blockage error at maximum angle of attack is evaluated through the cross-sectional model area as equal to 0.4% (Pope and Harper 1966), so that the total blockage error on the free-stream velocity is around 5% (0.005), *i.e.* smaller than measurement errors. In addition, the use of an open test section avoids the effect of growing boundary layers on the wind tunnel walls.

Two types of measurements have been performed, *i.e.* global forces acting on the wing, expressed in terms of lift and drag coefficients, and detailed velocity measurements in the wake. The former are measured using a force balance connected to the model by a cylindrical strut, the error on force coefficient being evaluated as equal to $\pm 3\%$ at the maximum velocity.

For the velocity measurements, in order to get a high spatial resolution over a large measurement section, a planar particle image velocimetry (PIV) system has been employed. Measurements are performed on horizontal (x, z) planes and on two vertical (x, y) planes in order to catch the three-dimensional nature of the phenomenon, both at bumps and valleys locations, as shown in Fig. 2. Note that measurements on different planes are not performed simultaneously and that the measurement region is around 2.5 chords in each direction with around 170×130 vectors in each image. The light plane is generated by means of a double-pulsed YAG laser (Twin-Quantel, wavelength of 532 nm and maximum pulse energy of 250 mJ), equipped with a cylindrical lens and synchronized with a high-resolution cross-correlation camera (PCO 4000, 10 Mpx), equipped with a Nikon NIKKOR 50 mm f1/1.2 objective. Oil droplets generated by a Laskin nozzle atomizer are used as tracers, with a mean diameter around 2 μm and density around 9×10^2 kg/m^3. The Stokes time scale is around 10^{-4} s, which is sufficiently small to resolve the large scale of the investigated flow field (c_r/U_0 is around 10^{-2} s). Double-pulse images are analysed by means of LaVision Davis software with interrogation window size decreasing from 128×128 px down to 32×32 px with window overlapping equal to 75%. Therefore, the average spatial resolution of the vector field is one vector every 2 mm, corresponding to a vector spacing of 0.02 times the root chord, *i.e.* 50 vectors along the root chord. Data post-processing for outlier detection compares the obtained velocity components at each point with those of 9 neighbours, within 30% difference, followed by one replacement step based on 4 by 4 neighbours. The error level in these measurements is derived on the basis of the number of replaced vectors in instantaneous vector fields, in comparison with the total number of vectors. This ratio is usually around 0.5%, but it is increased up to 1% in fully separating conditions at large angles of attack. In order to derive statistical moments, 1000 instantaneous images are averaged. The image acquisition rate is around 10 Hz, so that data can be considered as statistically independent (Falchi et al. 2006; Falchi and Romano 2009).

3 Overall force coefficients

Force acting on the three tested wings is measured as a function of the angle of attack α, from $-6°$ to more than 25°, and results of these measurements are reported in Fig. 3 for lift, drag, and lift to drag ratio, together with reference results. Regarding the standard wing, lift coefficient (Fig. 3a) exhibits a stall around 9° and a maximum lift coefficient around 0.8 This is in only in partial agreement with previous investigations, the details of stall behaviour being of course dependent on each specific airfoil and wing design, as reported in Fig. 3. For example, Miklosovic et al. 2007 used full-span and semi-span models, this last one being only considered here, with a NACA 0020 airfoil section and an idealized representation of a humpback whale flipper, which can account for the observed differences in stall angle and maximum lift coefficients. On the other hand, results by Rostamzadeh et al. 2013 were obtained using two-dimensional airfoils with wavy or tubercle leading edge. Therefore, the increased performances of their lift coefficients in

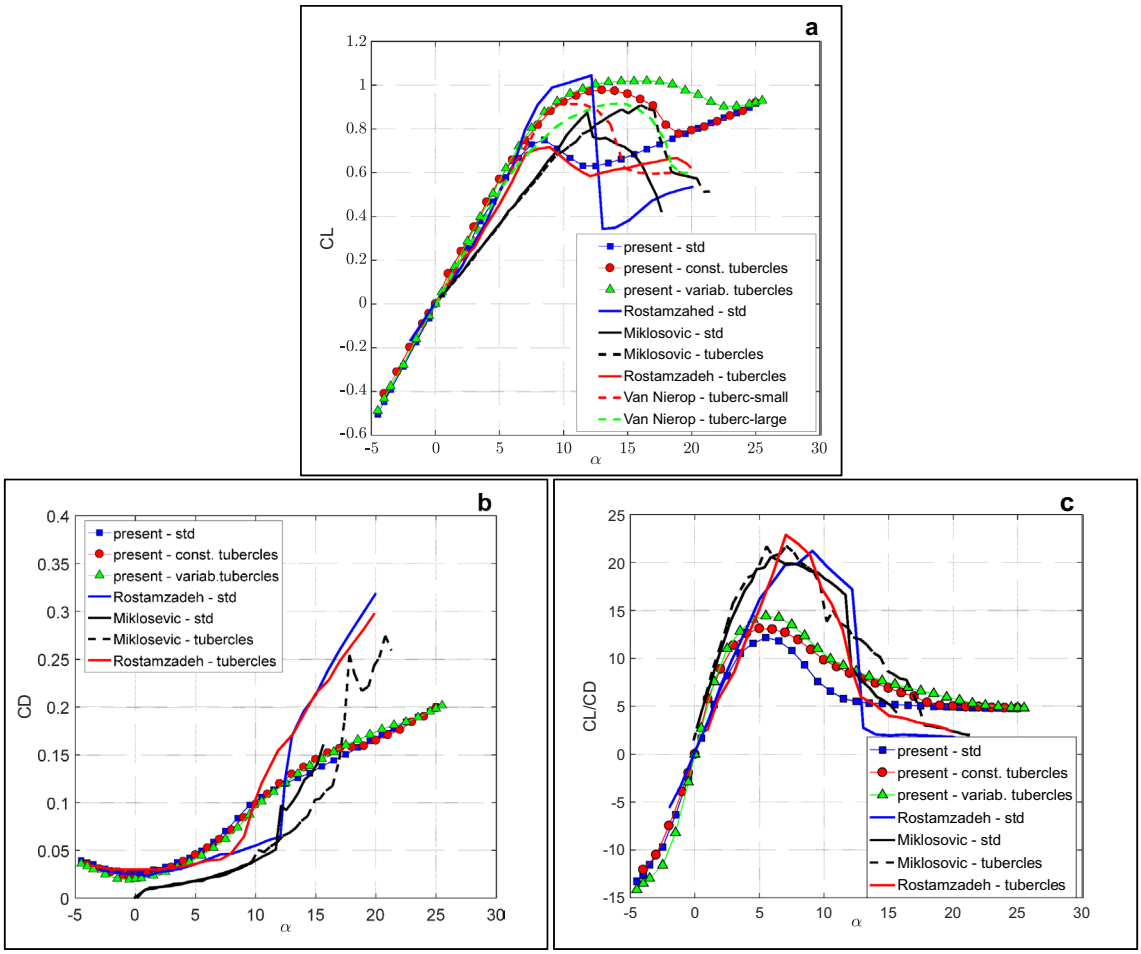

Fig. 3 Results from force measurements as a function of the angle of attack for the three tested wings (for error bars, see Fig. 4): lift coefficient (**a**), drag coefficient (**b**) and lift to drag ratio (**c**)

comparison with present data can be attributed to the difference between two-dimensional airfoils and three-dimensional wings.

For the present wing with tubercles of constant amplitude and wavelength, stall is delayed at around 13° with a maximum lift coefficient around 1, so far incremented of about 20%, with also a smoother pre- and post-stall behaviour in comparison with the standard wing. In comparison with reported references, again there are minor differences due to the specific geometrical details, but there is an overall common behaviour for tubercle wings, exhibiting a smoother stall, delayed to larger angles of attack and with a higher lift coefficient in comparison with standard wings at similar stall angles. This is especially true for the results by van Nierop et al. 2008, who used an elliptic wing with variable tubercle amplitudes, similar to the present wings.

The third tested wing, the one with tubercles of variable amplitude and wavelength, delays even forward the stall, up to 17°, so around 8° more than for the standard wing, with rather similar maximum lift coefficient, again in good agreement with results by van Nierop et al. 2008. The last results are obtained at variable tubercle amplitudes, $\eta = 0.05$ and $\eta = 0.12$, indicated in the figure as small and large tubercles, respectively, the first being very close to present data. So far, the present wing models with tubercles give substantial improvements in comparison with the standard wing, with simple leading-edge geometry and without major drawbacks far from stall.

Drag coefficients are reported in Fig. 3b and show rather similar trends before and after stall for the present standard wing and those with tubercles, even if there is a slight increase in drag for wings with tubercles after stall. The region at small angles of attack is also similar to the reference data by Rostamzadeh et al. 2013. On the other hand, the behaviour of these data around stall is strongly affected by the specific wing geometry and highly different from the present data, as also the data by Miklosovic et al. 2007, the last surely obtained on a more optimized profile to get low drag coefficient far from stall in comparison with the present one. From this point of view, it

is important to point out that the present cross section has been intentionally not optimized, in order to test performances of tubercles also on a rather rough geometry, to prove their effectiveness in all conditions.

Comparisons with results by Miklosovic et al. 2007, Van Nierop et al. 2008, and Rostamzadeh et al. 2013.

The actual impact of drag can be also evaluated by the lift to drag ratio, as presented in Fig. 3c. Here the performances of the present wing with variable tubercles are clearly superior to those of the standard wing and that with constant tubercles. In comparison with the results by Miklosovic et al. 2007 and Rostamzadeh et al. 2013, the lift to drag ratio of the present tubercle wings is definitely smaller in the angle of attack interval between 3° and 12°, whereas it is larger or comparable for larger angles of attack. In any case, a general result derived from all data, is that post-stall behaviour is improved by using tubercle wings in comparison with standard ones. Therefore, a net beneficial effect of the tubercle geometries is confirmed and this can be framed within a simplified non-viscous model as described in the following.

The argument is to consider these findings in terms of lift enhancement due to potential and vortex contributions, as introduced by Polhamus 1971, 1996, Mc Cormick 1994 and then reconsidered by Nelson and Pettier 2003. In addition to the usual potential contribution, this theory includes also an extra vortex contribution, which is relevant for low aspect ratio wings and specifically for delta wings. The idea under the application of this theory is that the specific design of the tubercles here adopted, *i.e.* small almost triangular elements at the leading edge of the wing, allows considering each tubercle contribution as that derived from a small delta wing. Following this line, the lift coefficient is given by (Bertin and Cummings, 2013 chapter 7.7 Eq. 7.61)

$$\begin{aligned} C_L &= C_{potential} + C_{vortex} \\ &= K_p \sin\alpha \cos^2\alpha + K_v \sin^2\alpha \cos\alpha = (1a) + (1b), \end{aligned} \quad (1)$$

where α is the angle of attack and (K_p, K_v) are coefficients dependent on the wing aspect ratio, to be determined empirically for each specific planform. Typical values for those coefficients are $K_p \approx (0.5 - 3)$, $K_v \approx (2 - 5)$, as reported by Polhamus, 1971 and Bertin and Cummings, 2013. The vortex lift contribution derives from the tip vortex typical of finite-span wings, which gives a relevant induced vertical velocity (downwash) on the wing itself, allowing reattachment of the flow even at high angles of attack. A tubercle wing is supposed to develop several pairs of tip vortices, each one from a single tubercle, extending downstream over the whole wing. This mechanism will be reconsidered in detail in the presentation and analysis of PIV velocity measurements.

Meanwhile, regarding force measurements, the lift coefficients presented in Fig. 3 are reconsidered in Fig. 4, including the potential and vortex contributions to lift, (1*a*) and (1*b*) in relation (1). For computations, the values $K_p = 0.5$ and $K_v = 2.5$ are used, as derived by best fitting to the present experimental data, the presence of multiple delta wings being just retained in the values of these coefficients. Error bars on measured coefficients have been included in this figure, whereas error bars are not included in Fig. 3 to avoid mismatching. In Fig. 4a, the almost linear part of all wings is well approximated by the potential lift contribution (1*a*),

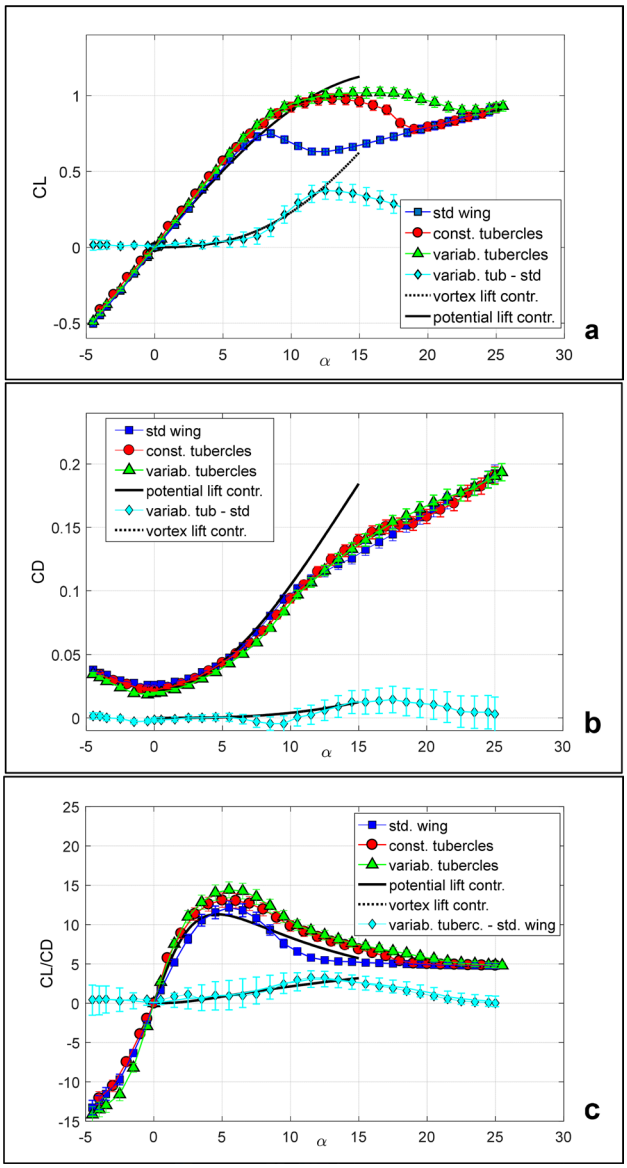

Fig. 4 Comparison of present results (with error bars) for the three tested wings with the proposed model as a function of the angle of attack: lift coefficient (**a**), drag coefficient (**b**), and lift to drag ratio (**c**). Potential lift (thick black line), vortex lift (dashed line), and difference between wings with tubercles and standard (in cyan)

while the difference between lift coefficients obtained for wings with variable tubercles and standard one (in cyan) is well approximated by the vortex lift contribution (1*b*). Of course, this is observed only before the stall, after that viscous contributions are also involved, which are not considered in Polhamus theory. Surely this explanation of tubercles acting as "small delta wings" developing tip vortex lift merits more detailed investigations.

Regarding drag coefficient, Polhamus theory leads to a relation similar to the previous one, *i.e.*

$$C_D = C_L \tan\alpha = K_p \sin^2\alpha\cos\alpha + K_v \sin^3\alpha = (2a) + (2b) \quad (2)$$

These contributions being added to the drag coefficient when $C_L = 0$, *i.e.* C_{D0}. Even in this case, as reported in Fig. 4b, the potential contribution (2*a*) well approaches the drag coefficient of standard wing, while vortex contribution (2*b*) seems to explain the observed differences among wings with variable tubercles and standard one. However, for drag force, the observed differences are so small that they can be retained within measurement errors. Lastly, in Fig. 5c, the lift to drag ratio is reported and compared to the model. Also in this case the measured values for the standard wing are well reproduced by the potential contribution, whereas the vortex contribution accounts for the larger part of the difference between the standard wing and the tubercle wing.

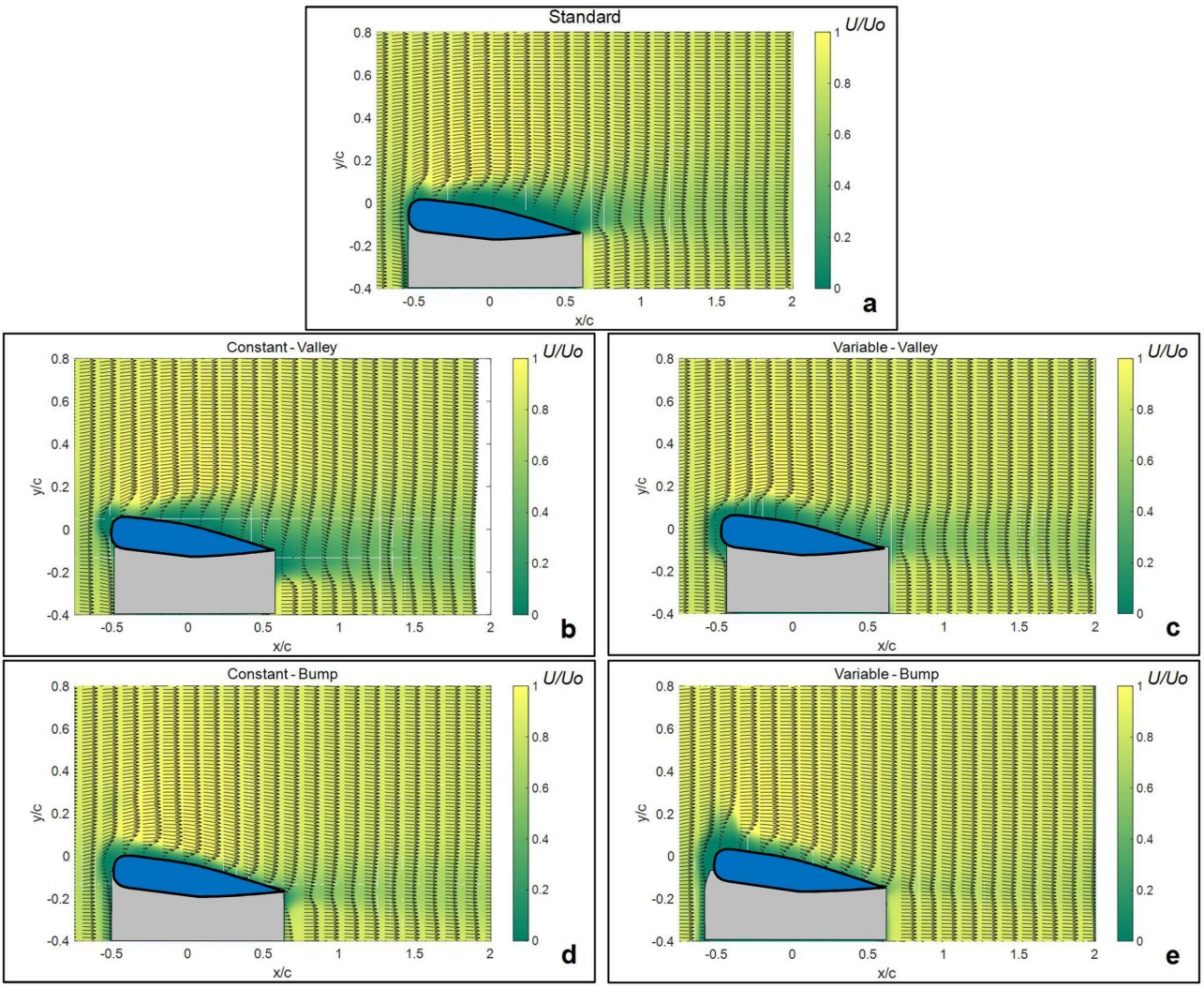

Fig. 5 Mean vector fields overlapped to non-dimensional streamwise velocity contours, for vertical measurement planes at an angle of attack equal to 5°. Standard wing (**a**), tubercle wings at the valley, constant (**b**) and variable (**c**), and tubercle wings at the bump, constant (**d**) and variable (**e**). Flow from left to right. The vertical axes and wings are stretched of a factor 1.5 to the horizontal

4 Detailed flow velocity fields: vertical planes

The results on forces acting on tubercle wings pointed out a possible mechanism to explain enhanced performances in terms of pairs of counter-rotating vortices, as in delta wings, and this claims for detailed local investigation of the velocity fields. These measurements are performed on planes orthogonal and parallel to the wing section, at three angles of attack, (5°, 10°, 15°), *i.e.* in the linear lift coefficient region, in the stall region, and in post-stall condition, as derived from Figs. 3 and 4. The results in full lift conditions for all wings, $\alpha = 5°$, are reported in Fig. 5. For a better representation of results, note that vectors are under-sampled by a factor 8 along the horizontal and that the vertical axis is stretched by a factor two in comparison with the horizontal, as also the wing thickness.

In this figure, five vector plots with overlapped streamwise velocity colours are presented, referring to the vertical plane at around 2/3 of the wing span both at tubercle bump and in the space between two tubercles, a valley, as reported in Fig. 2. For the standard wing (Fig. 5a) and for wings with tubercles at valley locations (Fig. 5b and c), the flow is attached without major recirculation, showing a reduced extension of the low-velocity region and a small velocity defect in the wake. The regions of reduced streamwise velocity correspond to the dark green colours in the figures. On the other hand, when results on bumps are considered, the extensions of the low-velocity regions on the wing and in the wake are considerably reduced for both constant and variable tubercle conditions (Fig. 5d and e).

This is an indication of different flow configurations depending on the local leading-edge geometry. The observed differences between flow passing over bumps or valleys suggest the presence of a cross-action among the two and therefore of relevant transverse motions, developing from the leading-edge downstream along the wing upper surface. However, at such a small angle of attack, the effect on wing performances is still small, even if improvements due to tubercles can be already observed in lift to drag ratio, as reported in Fig. 4c.

When the angle of attack is increased to 10°, these differences are still observed (not shown), but the most relevant results are obtained in full stall conditions for the standard wing, as reported in Fig. 6 for an angle of attack $\alpha = 15°$. In all conditions, stall is observed in the form of large regions of low streamwise velocities on the upper side of the wings and of large wake defects. However, the extension of such a recirculation is reduced for the wings with tubercles, especially at bump locations. In particular, the configuration with the smallest extension is that with variable tubercles at the bump, where a partial attachment is still observed in the form of a reduced low-velocity region (in Fig. 6e).

A more detailed evaluation of differences among tested geometries is derived by considering vertical profiles of streamwise velocity at different locations and different angles of attack. Specifically, profiles on the upper wing surface located at one-half of the chord are reported in Fig. 7, whereas profiles in the wake at one-half chord downstream are considered in Fig. 8. Regarding the former, at an angle of attack equal to 5° (Fig. 7a), all profiles show a positive velocity gradient at the wing surface ($y = 0$), so far indicating that separation does not occur at this angle of attack in all conditions. However, the trend towards external flow conditions exhibits some difference, being quicker for the constant tubercles at bump location, *i.e.* a thinner boundary layer, and slower for the variable tubercles at valley location, *i.e.* thicker boundary layer, the others being very similar. On the other hand, for an angle of attack equal to 10° (Fig. 7b), the standard wing and that with constant tubercles (at valley location) already show regions with backward flow close to the wing surface, as indicated by the negative velocity and velocity gradient close to the wing surface. Lastly, for $\alpha = 15°$ (Fig. 7c), all configurations show backward flows, more or less extended, except for the wing with variable tubercles at bump location. As a consequence, the velocity gradients at the wing surface are always negative, except for this last case. It is also important to remark that shear layers are in all conditions closer to the wing surface in comparison with the standard case, as also at an angle of attack of 10°, thus indicating a reduced flow separation region in comparison with the standard wing, as depicted in Fig. 6.

The velocity profiles in the wake, at one-half chord from the trailing edge are shown in Fig. 8. At an angle of attack of 5° (not shown), the velocity defects are quite small and similar in all conditions. For $\alpha = 10°$ (Fig. 8a), all velocity defects have large amplitude and intensity, down to 60–20% of the free-stream velocity, reaching negative velocities for $\alpha = 15°$ (Fig. 8b), except for the wing with variable tubercles both at valley and bump locations. The intensity and amplitude of this defect are responsible for the degradation of performances observed in lift and drag coefficients, to a minor extent for the variable tubercle configuration. This is an indication that the variable tubercle geometry allows improving wing performances, due to redistribution of local velocities and pressures, so far changing the overall force acting on the wing. The details of this process can be further investigated by considering the flow fields on a plane parallel to the wing surface.

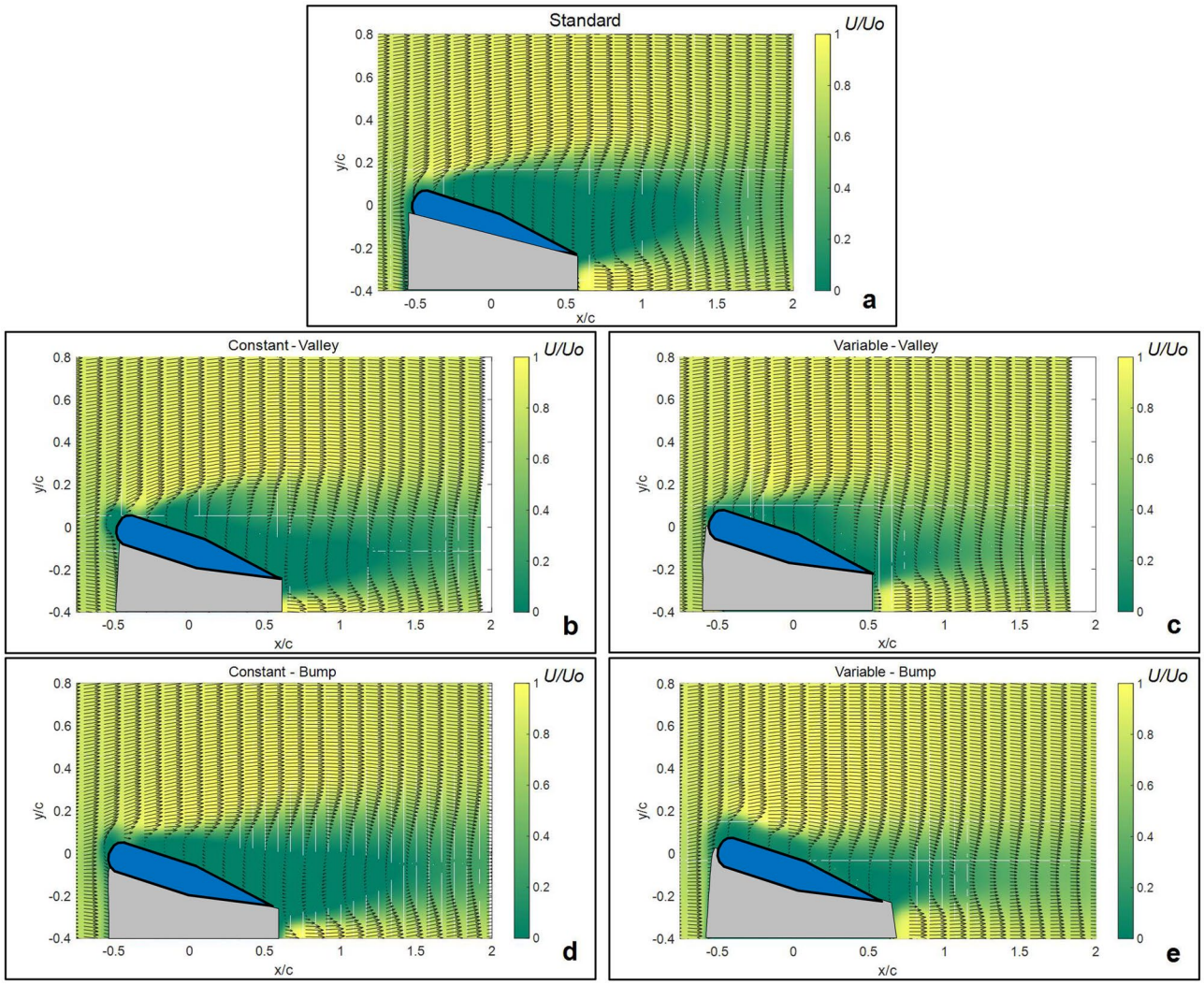

Fig. 6 Mean vector fields overlapped to non-dimensional streamwise velocity contours, for vertical measurement planes at an angle of attack equal to 15°. Standard wing (**a**), tubercle wings at the valley, constant (**b**) and variable (**c**), and tubercle wings at the bump, constant (**d**) and variable (**e**). Flow from left to right. The vertical axes and wings are stretched of a factor 1.5 to the horizontal

5 Detailed flow velocity fields: horizontal planes

The results on horizontal planes are presented in the following figures. Specifically, in Fig. 9 the streamwise velocity fields obtained for an angle of attack of 5° are reported. They confirm oil flow visualization made by Zhang et al. 2014, showing relevant wake defects downstream valley locations for wings with tubercles. Indeed, in the constant tubercle case (Fig. 10b), the defects are more persistent downstream, with a rather similar configuration when moving towards the tip in comparison with the variable tubercle condition (Fig. 10c), in which defects have lower and less persistent intensity. In addition, for this last condition, the distribution of velocity variation is definitely less uniform than before. For both tubercle wings, local accelerations downstream bumps are observed in addition to local decelerations downstream valleys, again especially for the constant tubercle condition. So far, at this angle of attack, the almost unaffected global behaviour between tubercle and standard wings, is the result of an average between local improvements and reductions of performances, in the form of accelerations over bumps and decelerations over valleys.

This effect can be made more quantitative by considering streamwise velocity profiles along the wing span, as presented in Fig. 10, at one-half chords downstream of the trailing edge. For the constant tubercle wing, the recurring velocity defects are uniformly distributed along the span, with increasing intensity towards the tip, in comparison with the almost flat behaviour observed for the standard wing. On the other hand, as already noticed, for variable tubercles, the intensity of defects is lower than for constant ones. In

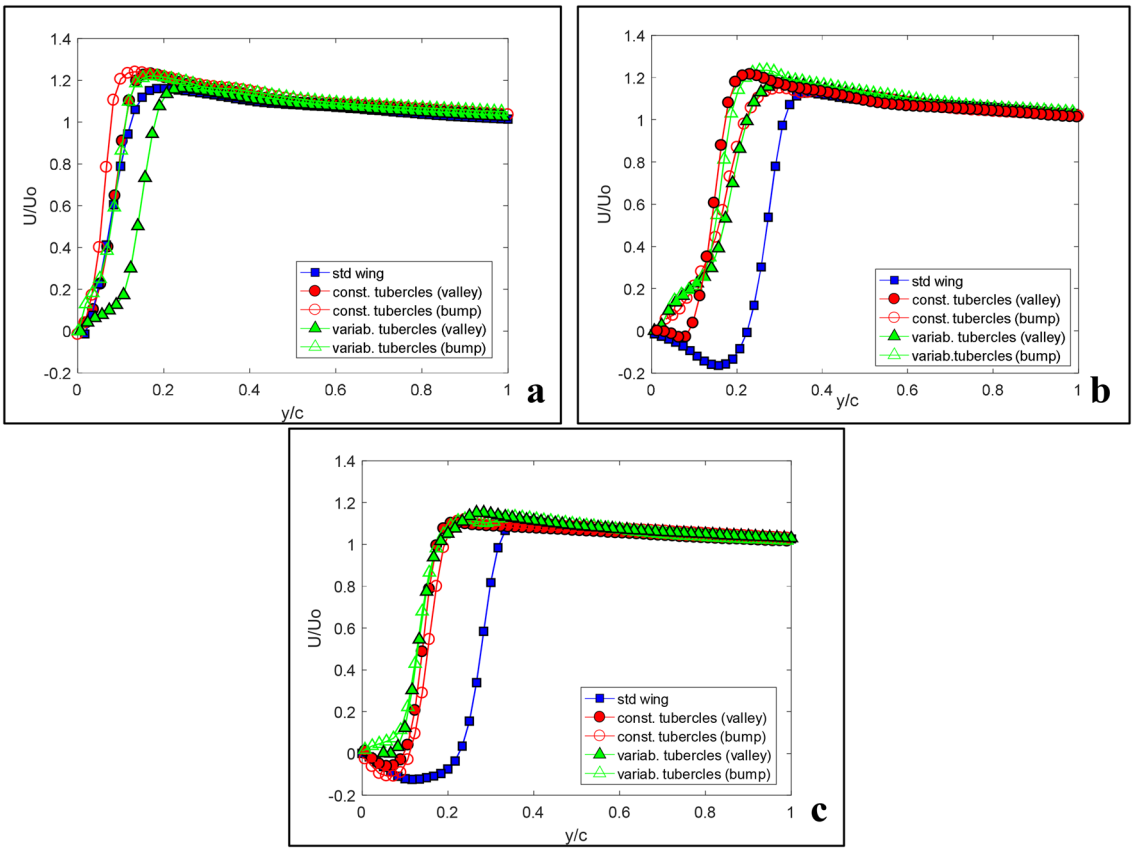

Fig. 7 Mean streamwise velocity profiles as derived one-half chord from the leading edge on the wing surface (indicated by $y/c = 0$), for the different tested geometries, at different angles of attack, $\alpha = 5°$ (**a**), $\alpha = 10°$ (**b**) and $\alpha = 15°$ (**c**)

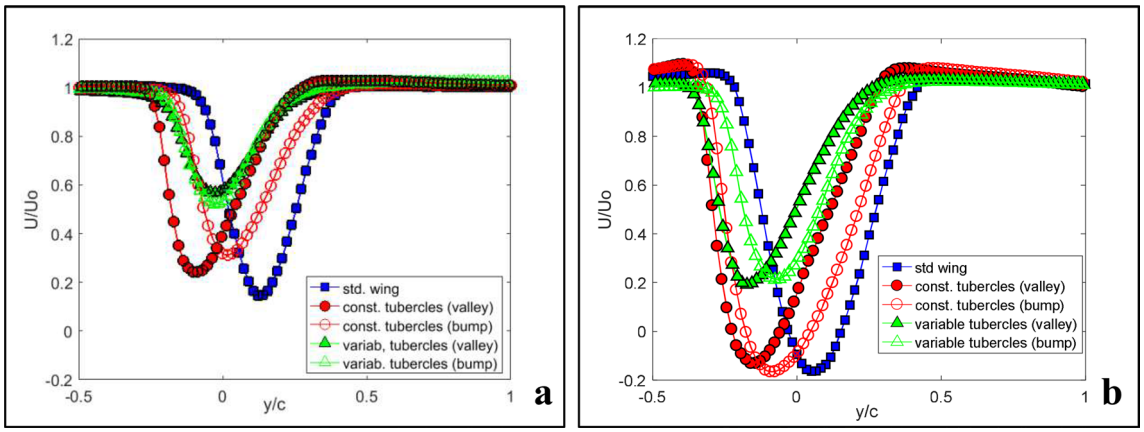

Fig. 8 Mean streamwise velocity profiles as derived one-half chord downstream of the trailing edge, for the different tested geometries, at different angles of attack, $\alpha = 10°$ (**a**) and $\alpha = 15°$ (**b**)

addition, the local velocity increments for the constant tubercle wing are also much higher than those for the variable tubercle wing, with also a more uniform spanwise distribution. So far the velocity difference between local velocity defects, located at valleys, and velocity increments, located at bumps, is reduced for the variable tubercle wing in comparison with the constant one.

It is useful to look at the average vorticity fields on this horizontal plane, as derived from average velocity and shown in Fig. 11. This helps understanding that each

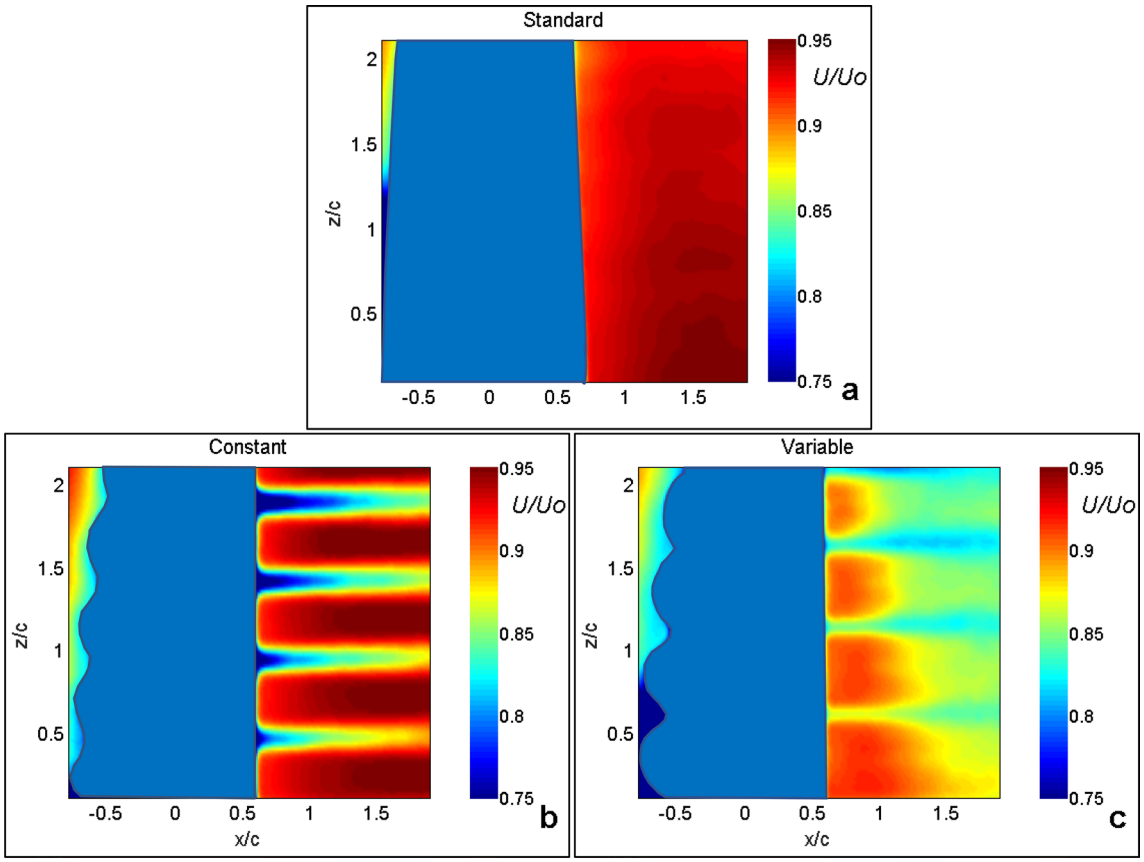

Fig. 9 Mean non-dimensional streamwise velocity contours, for horizontal measurement planes at an angle of attack equal to 5°. Standard wing (**a**), constant tubercle wing **b**, and variable tubercle wing (**c**). Flow from left to right. The coordinate $z/c = 0$ identifies the wing root

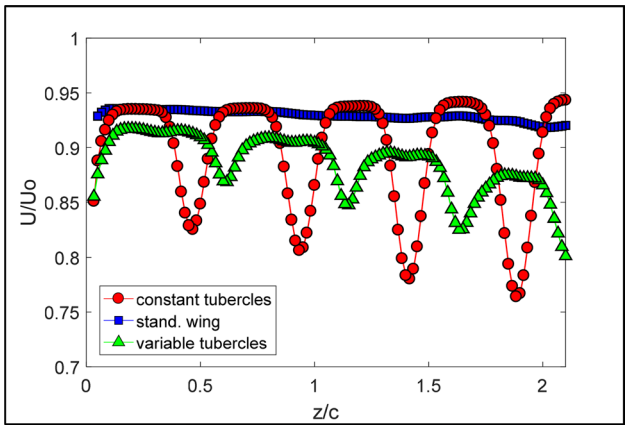

Fig. 10 Mean streamwise velocity profiles along the wing span at a distance equal to one-half chord downstream of the trailing edge as derived from horizontal measurement planes, at an angle of attack equal to 5°. The coordinate $z/c = 0$ identifies the wing root

bump is acting as a small delta wing, thus generating two counter-rotating vortices. These vortices interact with the similar ones coming from nearby bumps and move downstream along valleys. So far, they are supposed to induce local vertical and transverse velocities in opposite directions. These induced vertical velocities are just those contributing to flow attachment and lift increment observed on vertical planes at bump positions, as in Fig. 5d and e. In addition, in Fig. 11, for the case of variable tubercles, the maxima and minima of vorticity are still observed downstream valley positions, but in this case their intensity and distribution are reduced and much less uniform than for the case of constant tubercles. This effect leads to a slight reduction of the wake defect and drag coefficient in comparison with the constant tubercle condition, so that lift to drag ratio of the wing with tubercles will be superior to that of the standard one, as reported in Figs. 3 and 4.

As noticed, the vorticity fields of Fig. 11, claim for possible transverse velocities, which are reported in Figs. 12 and 13, respectively, for mean transverse velocity maps and mean transverse velocity profiles, at angles of attack of 5° and 15°. For the standard wing without tubercles at both 5° and 15° (Fig. 12a and d), the transverse velocity shows two large regions of opposite sign, with positive values towards the tip, for $z/c > 1.5$, and negative values towards the root, for $z/c < 0.5$ (indicated by the arrows in Fig. 12a and b). On the other hand, the wings with tubercles at an

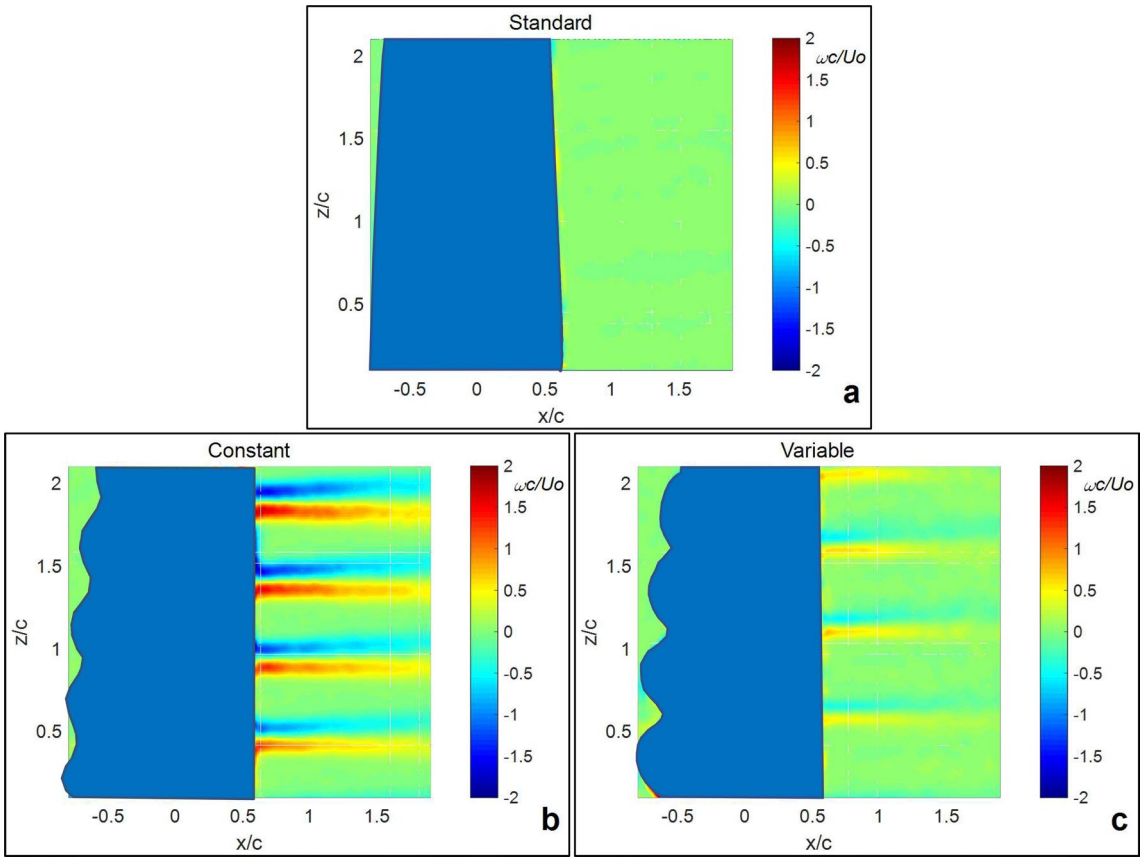

Fig. 11 Mean non-dimensional vorticity contours, for horizontal measurement planes at an angle of attack equal to 5°. Standard wing (**a**), constant tubercle wing (**b**), and variable tubercle wing (**c**). Flow from left to right. The coordinate $z/c = 0$ identifies the wing root

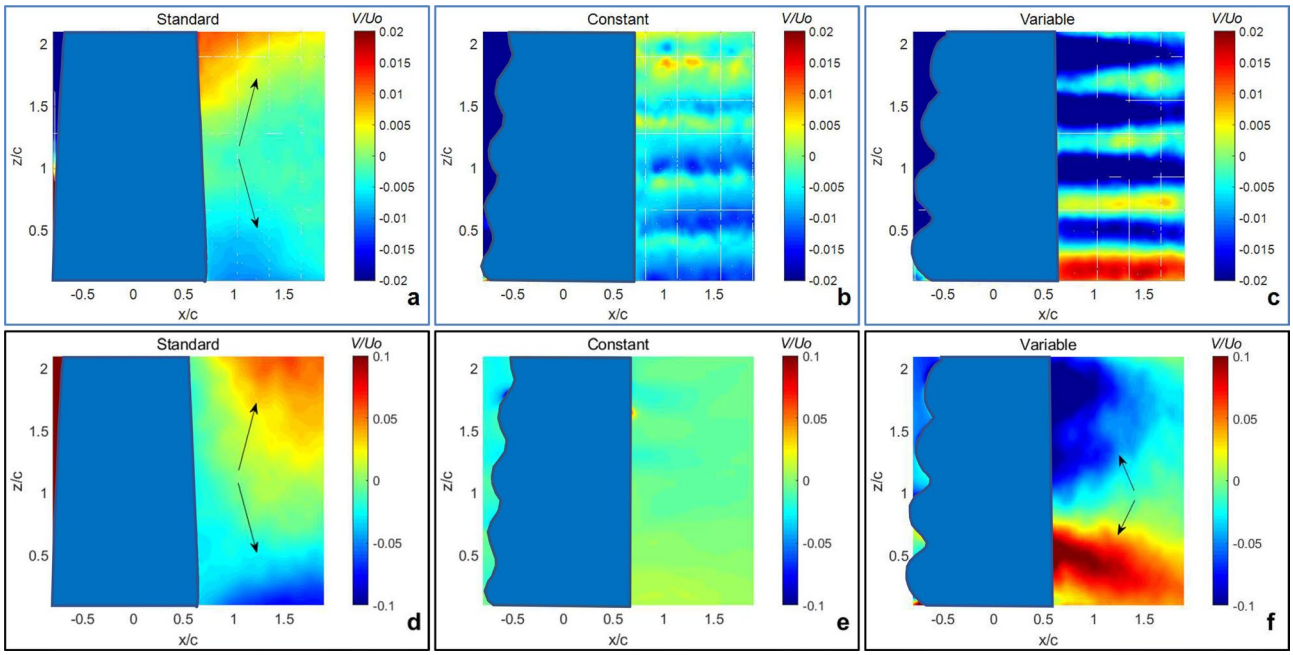

Fig. 12 Mean non-dimensional transverse velocity contours, for horizontal measurement planes at an angle of attack equal to 5° (at the top) and 15° (at the bottom). Standard wing (**a**) and **d**, constant tubercle wing (**b**) and (**e**), and variable tubercle wing (**c**) and (**f**). Flow from left to right. The coordinate $z/c = 0$ identifies the wing root

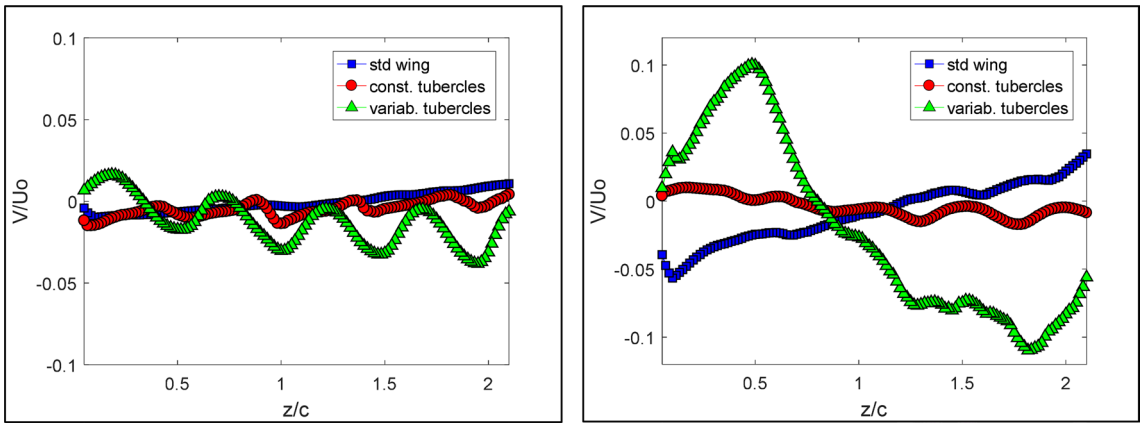

Fig. 13 Mean transverse velocity profiles along the wing span at a distance equal to 0.5 chord downstream of the trailing edge as derived from horizontal measurement planes, at an angle of attack equal to 5° (on the left) and 15° (on the right). The coordinate z/c = 0 identifies the wing root

angle of attack equal to 5° (Fig. 12b and c), point out a well-defined pattern, in the form of alternating bands of transverse velocity with opposite sign. These bands have an absolute value which is not constant along the span and it is higher for the wing with variable tubercles. Therefore, it seems that this last wing is able to generate more relevant transverse motions in comparison with the standard and constant tubercle wings. This is in agreement with results obtained for mean streamwise velocity and vertical vorticity (Figs. 9 and 11). At an angle of attack of 15°, the variable tubercle wing exhibits two large regions of opposite sign in comparison with the standard wing (indicated by arrows in Fig. 12f), whereas the constant tubercle wing still shows only a weak footprint of the previous band pattern (Fig. 12e). These considerations are made more quantitative by the analysis of transverse velocity profiles presented in Fig. 13.

At an angle equal to 5°, the standard wing presents slightly negative transverse velocity close to the root (z/c = 0) and slightly positive ones close to the tip, both in the order of 0.01 U_0. The two wings with tubercles show larger values of transverse velocity, modulated by the presence of the tubercles themselves, especially for the variable case. This situation is even more evident in terms of global transverse motions, when the angle of attack is equal to 15°, the absolute value being around 0.05 U_0 for the standard wing and 0.1 U_0 for the wing with variable tubercles. On the other hand, the situation is substantially unchanged for the constant tubercle geometry, showing the same regular pattern as at the smaller angle of attack. This indicates that the constant tubercle wing is not able to generate transverse motions as relevant as those generated by the variable tubercle wing. So far, from previous results, it is clear that tubercles of constant or variable length generate, especially at bump locations, local vertical and transverse motions affecting local and global performances of the wings, as in small delta wings.

6 Turbulence production and flow reattachment

So far, the analysis of the transverse velocities shades light into the possible additional generation of circulation on transverse planes, due to the presence of tubercles acting as small delta wings, which could explain the additional lift obtained from balance measurements. From the same balance measurements, also small reductions of drag and increments of lift to drag ratio are observed in presence of tubercles. It is important to relate such reduced drag also to fluctuating velocity fields and turbulence production by considering second-order statistics obtained from vertical plane measurements. Possible modified levels of fluctuations and turbulence, induced by the presence of tubercles, could be a concurrent factor in reducing the amplitude of the separation and of the wake, as previously observed on mean fields, so far reducing form drag (Pershin et al. 2020). To this end, in Figs. 14 and 15 the mixed turbulent stresses, *i.e.* the average product of fluctuating longitudinal and vertical velocities, on vertical planes are reported for the different investigated geometries, at angle of attacks equal to 5° and 15°, respectively. For $\alpha = 5°$, a large region of production of turbulence stresses on the upper side of the standard wing (Fig. 14a) and a layer of lower intensity and thickness generated from the bottom are clearly observed. In comparison with this condition, wings with tubercles show much lower levels of average cross-fluctuations in all conditions, on a minor extent for the wing with constant tubercles at valley location (Fig. 14b). Certainly, for the variable tubercle wing, both at valley and bump locations (Fig. 14c and e), turbulent

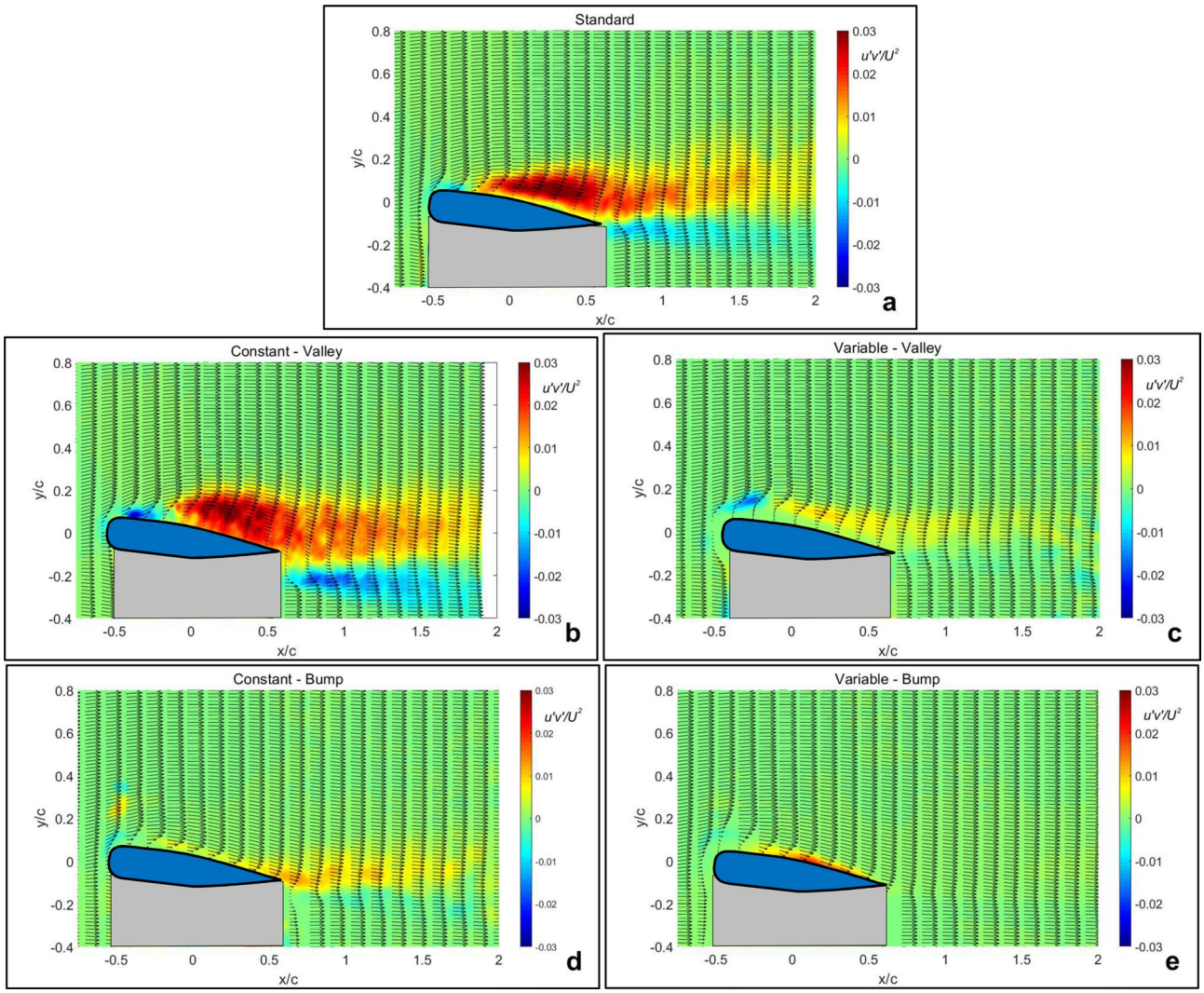

Fig. 14 Mean vector fields overlapped to non-dimensional Reynolds stress colour contours, for vertical measurement planes at an angle of attack equal to 5°. Standard wing (**a**), tubercle wings at the valley, constant (**b**) and variable (**c**), and tubercle wings at the bump, constant (**d**) and variable (**e**). Flow from left to right. The vertical axes and the wings are stretched of a factor 1.5 to the horizontal

stress levels and consequently turbulence production are lower than in the standard wing, as also at bump locations, in both constant and variable tubercle conditions (Fig. 14d and e).These results are in agreement with the extensions of recirculating and wake defect regions observed on mean fields, reported in Fig. 5.

When the angle of attack is increased up to 15°, as reported in Fig. 15a, as expected, the standard wing is exhibiting two strong shear layers, generated from leading and trailing edges, with high levels of turbulent stresses, of opposite sign, associated with the boundaries of the large separation region. For the tubercle wings, the situation is similar, but in general the intensity of fluctuations seems smaller and the position of the upper shear layers is closer to the wing in comparison with the standard wing. This is especially true for the wing with variable tubercles at bump locations (Fig. 15e). As remarked, this result has to be retained in parallel to the reduced extension of the separation region, as obtained in average fields.

7 Discussion and concluding remarks

This work is focused on the aerodynamic field generated over a wing/blade in which the leading edge is modified by the presence of artificial undulation, following examples in nature ("biomimetics"). Specifically, artificial tubercles inspired by those observed in humpback whales are considered, by focusing on the effects of their wavelength and amplitude on the flow field, in comparison with the standard wing without any tubercle, used for comparisons. Starting from previous observations, in which the use of leading-edge

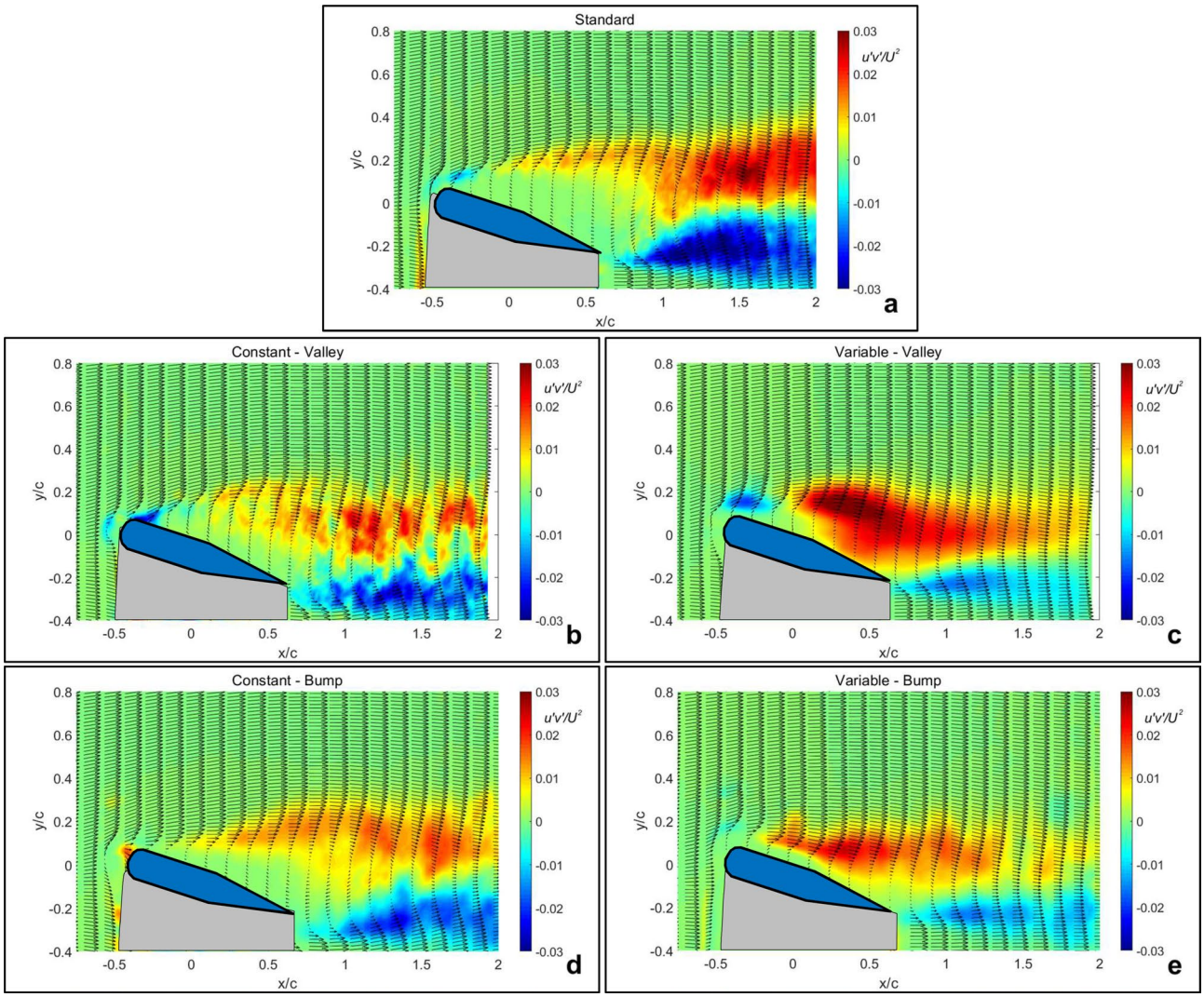

Fig. 15 Mean vector fields overlapped to non-dimensional Reynolds stress colour contours, for vertical measurement planes at an angle of attack equal to 15°. Standard wing (**a**), tubercle wings at the valley, constant (**b**) and variable (**c**), and tubercles wing at the bump, constant (**d**) and variable (**e**). Flow from left to right. The vertical axes and the wings are stretched of a factor 1.5 to the horizontal

tubercles resulted to be beneficial, independently of the specific geometry adopted, the idea is to consider easy manufacturing and simple solutions to be used for technological applications.

The approach is experimental by measuring both overall forces acting on the wings and local velocity fields around the wings, to determine phenomena and mechanisms involved. The present wings equipped with tubercles, in comparison with a standard wing allow to:

- Increase the maximum lift coefficient of around 20% and delay the stall angle of about 4°, with a smoother pre- and post-stall behaviour and simultaneously keeping drag coefficients almost unchanged, so far leading to a net increase in lift to drag ratio (this is reported in Fig. 3);
- Reduce the extension of the small velocity region on the upper side of the wing, especially when the angle of attack is closer or larger to stall, in a more evident way for the case of the wing with tubercles of variable wavelength and amplitude and more over tubercle bumps rather than over valleys (this is reported in Figs. 5 and 6);
- Avoid separation and backflow on the wing upper surface and reduce velocity defect in the wake, close and over stall angle, again especially for the wing with variable tubercles over bumps (reported in Figs. 7 and 8);
- Produce a spanwise wake pattern with bands of reduced and increased streamwise velocities, corresponding to similar bands of alternate sign of vorticity, quite regular and uniform for the constant tubercle wing and more irregular for the variable tubercle wing (Figs. 9, 10, 11);

- Generate a global large-scale transverse motion around the wing and in the wake, which is added to the tip vortex, as revealed by the investigation of transverse velocities, the effectiveness and intensity of this motion being much higher for the variable tubercle wing, especially at large angles of attack (Figs. 12 and 13);
- Reduce the level of turbulence production and the distance between shear layers, again especially in the case of variable tubercle, at bump locations (Figs. 14 and 15).

The arguments to explain the overall observed behaviour are here reported in terms of a simplified non-viscous model in which lift enhancement is due to vortex contributions (Polhamus 1971, 1996; Nelson and Pettier 2003), to be added to the usual potential contribution, as in delta wings. In some sense, the specific design of the tubercles here adopted, consisting of small almost triangular elements at the wing leading edge, allows considering each tubercle contribution as a small delta wing generating pairs of counter-rotating tip vortices. These vortices induce vertical and transverse velocities over the wing, which reduce separation and leading-edge stall for increasing angles of attack. This picture is confirmed by verifying predictions of the simplified model with experimental data (as shown in Fig. 4).

Detailed local fields also allow distinguishing differences between constant and variable tubercle geometries. The last perform definitely more efficiently in generating transverse motions at leading-edge bump locations, in the form of two pairs of counter-rotating vortices, as in small delta wings. These interact along valleys and originate local induced transverse and velocities, contributing to flow reattachment and lift increment. So far, the use of tubercles with almost triangular bump form, with variable amplitude and wavelength, generates additional induced motion and velocities, thus allowing optimizing performances in specific operative ranges.

The present analysis must be extended to the evaluation of flow fields and performances in unsteady conditions when preliminary indications suggest an even better situation in comparison with standard wings.

Acknowledgements The authors would like to thank Massimo Falchi, Paolo Mondati, Giuseppe Sisinni, and Domenico Pietrogiacomi for the help in acquiring data and images.

Authors' contribution G.P.R contributed to conceptualization. All authors contributed to methodology, data curation, and data visualization and also contributed equally to writing the paper and reaching conclusions. They all approved the final submitted draft.

Funding Open access funding provided by Università degli Studi di Roma La Sapienza within the CRUI-CARE Agreement. The activities have been funded by Sapienza University in the framework of a project on Unsteady and advanced aerodynamics-Progetti di Ricerca Medi-2019.

Data availability Data and material are available on request to the corresponding author.

Code availability Not applicable.

Declarations

Conflicts of interest The authors report no conflict of interest.

References

Anders, JB (2000) Biomimetic flow control. In: AIAA paper, p. 2543 https://doi.org/10.2514/6.2000-2543

Bertin JJ, Cummings RM (2013) Aerodynamics for engineers, 5th edn. Pearson Prentice Hall, New Jersey

Bolzon MD, Kelso RM, Arjomandi M (2016) Tubercles and their applications. J Aerosp Eng 29:04015013

Bolzon MD, Kelso RM, Arjomandi M (2017) Performance effects of a single tubercle terminating at a swept wing's tip. Exp Therm Fluid Sci 85:52–68

Chaitanya P, Josep P, Narayanan S, Vanderwel C, Turner J, Kim JW, Ganapathisubramani B (2017) Performance and mechanism of sinusoidal leading edge serrations for the reduction of turbulence–aerofoil interaction noise. J Fluid Mech 818:435–464

Chen H, Wang JJ (2014) Vortex structures for flow over a delta wing with sinusoidal leading edge. Exp Fluids 55:1761

Choi H, Hyungmin P, Woong S, Sang-im L (2012) Biomimetic flow control based on morphological features of living creatures. Phys Fluids 24:121302

Corsini, A, Delibra G, Sheard AG (2013) On the role of leading-edge bumps in the control of stall onset in axial fan blades. J Fluid Eng ASME, 135(8)

Custodio, D (2007) The effect of humpback whale-like LE protuberances on hydrofoil performance. In: Master of Science Thesis, Worcester Polytechnic Institute

Custodio D, Henoch CW, Johari H (2015) Aerodynamic characteristics of finite span wings with leading-edge protuberances. AIAA J 53(7):1878–1893

de Paula AA, Meneghini J, Kleine VG, Girardi RD (2017) The wavy leading edge performance for a very thick airfoil. In: 55th AIAA Aerospace Sciences Meeting, p. 0492

Falchi M, Querzoli G, Romano GP (2006) Robust evaluation of the dissimilarity between interrogation windows in image velocimetry. Exp Fluids 41(1):21–33

Falchi M, Romano GP (2009) Evaluation of the performance of high-speed PIV compared to standard PIV in a turbulent jet. Exp Fluids 47:509–526

Fish FE, Battle JM (1995) Hydrodynamic design of the humpback whale flipper. J Morphol 225:51–60

Fish FE, Lauder GV (2006) Passive and active flow control by swimming fishes and mammals. Annu Rev Fluid Mech 38:193

Fish FE, Weber PW, Murray MM, Howle LE (2011) The tubercles on the humpback whale flippers: application of bio-inspired technology. Integr Comp Biol 51:203–213

Goruney T, Rockwell D (2009) Flow past delta wing with a sinusoidal leading edge: near-surface topology and flow structure. Exp Fluids 47:321–331

Guan Y, Pröbsting S, Stephens D, Gupta A, Morris SC (2016) On the wake flow of asymmetrically beveled trailing edges. Exp Fluids 57:78

Hansen KL, Kelso RM, Dally BB (2010) An investigation of three-dimensional effects on the performance of tubercles at low Reynolds numbers. In: 17th Australasian fluid mechanics conference, p. 5–9, Auckland, New Zealand

Hansen KL, Kelso RM, Dally BB (2011) Performance variations of leading-edge tubercles for distinct airfoil profiles. AIAA J Aircraft 49:185–194

Hansen KL, Rostamzadeh N, Kelso RM, Dally BB (2016) Evolution of the streamwise vortices generated between leading edge tubercles. J Fluid Mech 788:730–766

Jansen JA, Nilsson J (2017) Application of a humpback whale fin as a rudder. In: Master's Thesis in naval architecture and ocean engineering, Chalmers University of Technology, Göteborg, Sweden

Johari H, Henoch C, Custodio D, Levshin A (2007) Effects of leading edge protuberances on airfoil performance. AIAA J 45:2634–2642

Kosma MM, Werth AJ, Szabo AR, Straley JM (2019) Pectoral herding: an innovative tactic for humpback whale foraging. Royal Soc Open Sci 6:191104

Li Z, Qian Z, Ji B (2020) Transient cavitating flow structure and acoustic analysis of a hydrofoil with whalelike wavy leading edge. Appl Math Model 85:60–88

McCormick BW (1994) Aerodynamics, aeronautics, and flight mechanics, 2nd edn. Wiley, New Jersey

Meng X, Abbasi AA, Li H, Yin S, Qi Y (2019) Bioinspired experimental study of leading-edge plasma tubercles on wing. AIAA J 57:462

Miklosovic DS, Murray MM, Howle LE, Fish FE (2004) Leading-edge tubercles delay stall on humpback whale flippers. Phys Fluids 16:L39–L42

Miklosovic DS, Murray MM, Howle LE (2007) Experimental evaluation of sinusoidal leading edges. J Aircr 44:1404–1407

Nelson RC, Pelletier A (2003) The unsteady aerodynamics of slender wings and aircraft undergoing large amplitude maneuvers. Prog Aerosp Sci 39:185–248

New DTH, Ng BF (2020) Flow control through bioinspired leading-edge tubercles: morphology, aerodynamics, hydrodynamics and applications. Springer Nature, Switzerland

Pendar MR, Esmaeilifar E, Roohi E (2020) LES study of unsteady cavitation characteristics of a 3D hydrofoil with wavy leading edge. Int J Multiph Flow 132:103415

Pendar MR, Páscoa JC (2022) Numerical investigation of plasma actuator effects on flow control over a three-dimensional airfoil with a sinusoidal leading edge. J Fluids Eng 144:081208

Pershin A, Beaume C, Tobias SM (2020) A probabilistic protocol for the assessment of transition and control. J Fluid Mech 895:A16

Polhamus EC (1971) Predictions of vortex-lift characteristics by a leading edge suction analogy. J Aircr 8(4):193–199

Polhamus EC (1996) A concept of the vertex lift of sharp-edge delta wings based on a leading-edge suction analogy. (NASA TN, D- 3767)

Pope A, Harper JJ (1966) Low-speed wind tunnel testing. Wiley, New York

Rostamzadeh N, Kelso RM, Dally BB, Hansen KL (2013) The effect of undulating leading-edge modifications on NACA 0021 airfoil characteristics. Phys Fluids 25:117101

Rostamzadeh N, Hansen KL, Kelso RM, Dally BB (2014) The formation mechanism and impact of streamwise vortices on NACA 0021 airfoil's performance with undulating leading edge modification. Phys Fluids 26:107101

Segre PS and other 17 authors (2020) Energetic and physical limitations on the breaching performance of large whales. eLIFE, **9**, e51760

Shanmukha Srinivas K, Datta A, Bhattacharyya A, Kumar S (2018) Free-stream characteristics of bio-inspired marine rudders with different leading-edge configurations. Ocean Eng 170:148–159

Shi W, Atlar M, Norman R, Aktas B, Turkmen S (2016) Numerical optimization and experimental validation for a tidal turbine blade with leading-edge tubercles. Renew Energy 96:42–55

Stanway, MJ (2008) Hydrodynamic effect of leading edge tubercles on control surfaces and in flapping foil propulsion. In: PhD Thesis, Massachusetts Institute of Technology

van Nierop E, Alben S, Brenner MP (2008) How bumps on whale flippers delay stall: an aerodynamic model. Phys Rev Lett 100:054502

Watts, P, Fish, FE (2001) The influence of passive leading edge tubercles on wing performance. In: Proceedings of 11th Int Symposium on Unmanned Untethered Submersible Technology, Durham, UK

Wei Z, New TH, Cui YD (2017) Aerodynamic performance and surface flow structures of leading edge tubercled tapered swept-back wings. AIAA J 56(1):423–431

Zhang MM, Wang GF, Xu JZ (2014) Experimental study of flow separation control on a low-Re airfoil using leading-edge protuberance method. Exp Fluids 55:1710